07.2

Monolithic triple-junction $p-i-n$ AlGaAs/GaAs laser photoconverter

© V.S. Kalinovskii, E.V. Kontrosh, I.A. Tolkachev, K.K. Prudchenko, S.V. Ivanov

Ioffe Institute, St. Petersburg, Russia
E-mail: vitak.sopt@mail.ioffe.ru

Received June 24, 2024
Revised July 20, 2024
Accepted July 25, 2024

The photovoltaic characteristics of heterostructural triple-junction $p-i-n$ AlGaAs/GaAs photoconverters of monochromatic radiation grown by molecular-beam epitaxy in a single technological process have been studied. The spectral sensitivity of the created triple-junction photoconverters was in the wavelength range $0.78-0.87\,\mu$m. The achieved values of open circuit voltage 1.82 V and electrical power $0.34\,\mathrm{mW/cm^2}$ in the photovoltaic mode at laser radiation power densities $\leqslant 2\,\mathrm{mW/cm^2}$ at a wavelength $\lambda = 850\,$nm exceed the characteristics of single-junction $p-i-n$ AlGaAs/GaAs photoconverters created by identical technology. The developed triple-junction photoconverters can be used in remote power systems for miniature microcircuits, in implantable bioelectronics and biosensors, as well as in long-term radioluminescent energy sources.

Keywords: molecular-beam epitaxy, triple-junction photoconverters, photovoltaic characteristics, laser radiation, $p-i-n$ AlGaAs/GaAs photoconverters, wavelength.

DOI: 10.61011/TPL.2024.11.59675.20031

Optical systems for wireless and fiber-optic transmission of energy and information [1–4], remote energy systems for submillimeter-scale sensor devices, bioimplantable devices [5–7], and long-term radioluminescent energy sources [8–11] require the development and construction of efficient photovoltaic converters (PVCs) of optical radiation. The efficiency of these systems is largely determined by the increase in voltage and electrical power generated by a PVC, a high signal-to-noise ratio, and the linearity of dependence of the current signal on the level of optical power transmitted from an optical source via a fiber-optic communication line. The engineering and fabrication of monolithic multi-junction photovoltaic converters (MJ PVCs) from photoactive subcells with the same band gap are promising in this regard [3]. The viability of MJ PVCs with up to 100 junctions was substantiated in literature [3–6]. The dimensions of layers of a multi-junction $p-i-n$ PVC are determined primarily by the wavelength and the coefficient of absorption of monochromatic radiation in the semiconductor material under the condition of equality of currents generated by light in each subcell. Expression

$$P_0(1-e^{-l_1}) = P_0 e^{-l_1-l_{td\_1}}(1-e^{-l_2}) = P_0 e^{-l_1-l_{td\_1}-l_2-l_{td\_2}}(1-e^{-l_3}) \quad (1)$$

represents the equality of monochromatic radiation absorption in each subcell, which ensures the equality of photocurrents. Equation (1) allows one to estimate the optical thicknesses in subcells of a monolithic triple-junction $p-i-n$ PVC. In (1), P_0 is the incident optical radiation intensity; $l_j = \alpha_{pj}h_{pj} + \alpha_{ij}h_{ij} + \alpha_{nj}h_{nj}$ $(j = 1, 2, 3)$ is the optical thickness of the first, the second, and the third subcells; $l_{td\_m} = \alpha_{ptd\_m}h_{ptd\_m} + \alpha_{ntd\_m}h_{ntd\_m}$ $(m = 1, 2)$ is the optical thickness of the first and the second connecting tunnel diodes; and h and α are the actual thicknesses and the absorption coefficients of p, i, and n layers of the first, the second, and the third subcells and the connecting tunnel diodes. A series connection of photoactive subcells through tunnel diodes in a monolithic MJ PVC structure allows for an increase in output voltage and electrical signal power at lower operating currents and ensures better matching with the load. The fabrication of fiber-optic modules containing several interconnected monolithic MJ PVCs should provide an opportunity to reduce the number of components in photovoltaic assemblies and suppress optical and electrical losses both in fiber-optic splitters and in intercomponent connections [12].

In the present study, we report the results of examination of photovoltaic characteristics of monolithic triple-junction $p-i-n$ AlGaAs/GaAs PVCs (TJ PVCs) (Fig. 1, *a*) in comparison with the characteristics of single-junction $p-i-n$ AlGaAs/GaAs PVCs (SJ PVCs) under excitation by continuous laser radiation with wavelength $\lambda = 850\,$nm at power densities $\leqslant 2\,\mathrm{mW/cm^2}$.

Triple-junction $p-i-n$ AlGaAs/GaAs PVCs were grown by molecular-beam epitaxy (MBE) on an n-GaAs $(N_D \sim 3\cdot 10^{18}\,\mathrm{cm^{-3}})$ substrate. The monolithic PVC structure (Fig. 1, *a*) included three $p-i-n$ GaAs subcells with the thicknesses of the upper $(\sim 0.4\,\mu\mathrm{m})$, middle $(\sim 0.7\,\mu\mathrm{m})$, and lower $(\sim 2.3\,\mu\mathrm{m})$ junctions chosen in accordance with expression (1) and the results of earlier calculations [12]. The doping levels were $N_A \geqslant 1\cdot 10^{18}\,\mathrm{cm^{-3}}$ for p layers, $N_D \leqslant 1\cdot 10^{18}\,\mathrm{cm^{-3}}$ for n layers, and $\sim 1\cdot 10^{15}\,\mathrm{cm^{-3}}$ for i layers. Back-to-back nanosized tunnel diodes based on $p^{++}-n^{++}$-GaAs (each with an overall thickness $\leqslant 30\,$nm) were used as connecting elements between the $p-i-n$ junctions. The structure included a wide-band p-$Al_{0.2}Ga_{0.8}As$ window (with

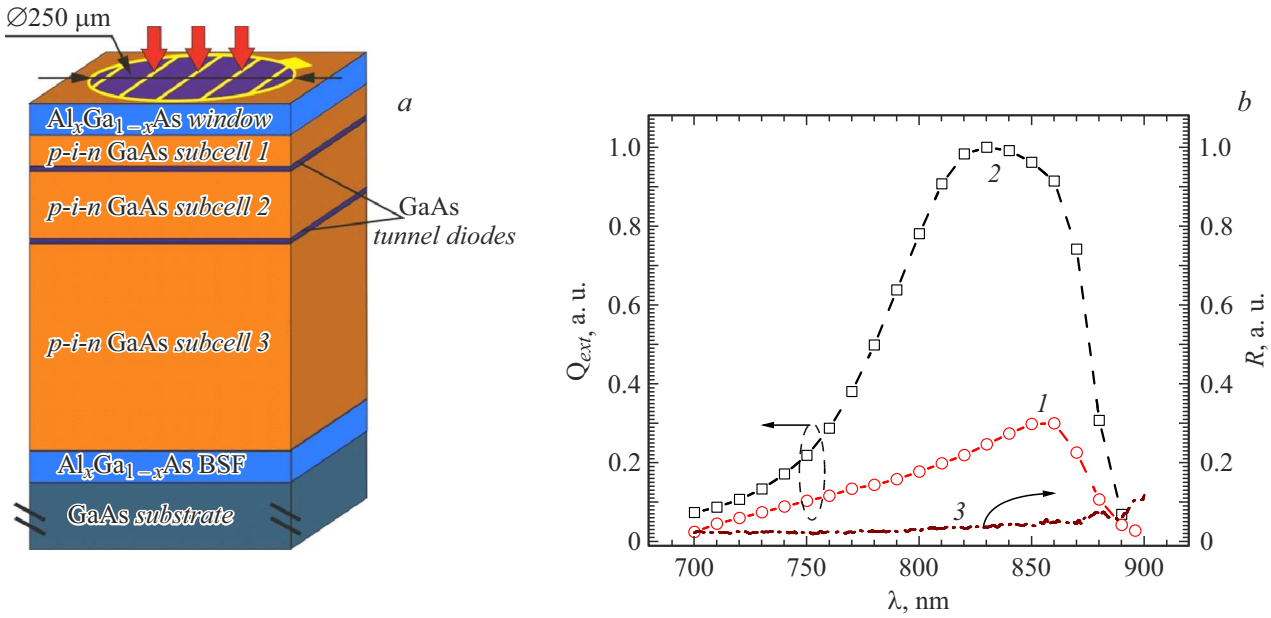

Figure 1. *a* — Monolithic triple-junction $p-i-n$ AlGaAs/GaAs PVC. The upper (*1*), middle (*2*), and lower (*3*) $p-i-n$ GaAs subcells and connecting tunnel diodes based on $n^{++}-p^{++}$-GaAs are indicated. *b* — Photosensitivity spectra of the triple-junction $p-i-n$ PVC (*1*) and the single-junction $p-i-n$ PVC (*2*). *3* — Coefficient of reflection from the photoactive surface of the triple-junction $p-i-n$ PVC.

$N_A \sim 5 \cdot 10^{19}\,\mathrm{cm}^{-3}$ and a thickness of $0.3\,\mu$m) and a back n-$Al_{0.2}Ga_{0.8}As$ potential barrier (with $N_D \sim 3 \cdot 10^{18}\,\mathrm{cm}^{-3}$ and a thickness of $0.2\,\mu$m). PVC chips with a photosensitive surface $250\,\mu$m in diameter, an Ag(Mn)/Ni/Au ring front contact with thickness $h = 3600$ Å, and an Au(Ge)/Ni/Au solid back contact with thickness $h = 2000$ Åwere formed by post-growth planar processing; the side surface of the structure was passivated with a Si_3N_4 dielectric layer. Note that the TJ PVC structure parameters determined using expression (1), specified in fabrication (Fig. 1, *a*), and estimated via secondary ion mass-spectrometry agree closely with each other. The deviation of layer thicknesses in the monolithic epitaxial TJ PVC heterostructure from the calculated ones did not exceed 12%.

Single-junction AlGaAs/GaAs PVCs used for comparison were grown by MBE [12] and formed using the same post-growth processing procedure with similar contacts and a photosensitive surface $250\,\mu$m in diameter. The photosensitivity spectra (Fig. 1, *b*), dark (Fig. 2, *a*) and light (Fig. 2, *b*) current–voltage curves (CVCs), and capacitance–voltage relationships (CVRs) (Fig. 2, *a*) of both types of PVCs were measured directly on the epitaxial wafer at room temperature. The dark CVCs of SJ and TJ PVCs were measured at a forward bias voltage up to 1.5 and 4 V, respectively. The external quantum efficiency characteristics of SJ and TJ PVCs were measured within the range from 700 to 900 nm using a high-aperture monochromator with optical signal input from a $50\,\mu$m optical fiber. The experimental dependences of normalized external quantum efficiency values for the TJ PVC (curve *1*) and the SJ PVC (curve *2*) are shown in Fig. 1, *b*. The external quantum efficiency at wavelength $\lambda = 850$ nm was $Q_{ext} = 80\%$ and $Q_{ext} \sim 30\%$ for SJ and TJ PVCs (Fig. 1, *b*), which is attributable to the redistribution of optical power in the TJ PVC between three $p-i-n$ subcells and the resulting proportional reduction in photocurrent in the monolithic triple-junction structure.

Calculated parameters obtained by fitting the forward dark CVCs of monolithic triple-junction and single-junction $p-i-n$ PVCs

$p-i-n$ PVC type	J_{0t}, A/cm^2	J_{0r}, A/cm^2	J_{0d}, A/cm^2	R_s mΩ · cm^2
Triple-junction	$1.1 \cdot 10^{-8}$	$5.3 \cdot 10^{-11}$	$2.6 \cdot 10^{-21}$	140
Single-junction	$7.1 \cdot 10^{-9}$	$5.1 \cdot 10^{-10}$	$5.6 \cdot 10^{-20}$	1.6

The dominant mechanisms of current transport and the values of saturation currents (J_{0i}) and diode coefficients (A_i) were determined by analyzing the experimental dark CVCs of triple-junction and single-junction PVCs. The transport mechanisms (see Fig. 2, *a* and the table) are as follows: tunnel-trap (J_{0t}; curves *3* ($A_t > 6$) and *8* ($A_t > 2$) for TJ and SJ PVCs, respectively); recombination (J_{0r}; curves *4* ($A_r = 6$) and *9* ($A_r = 2$ for TJ and SJ PVCs, respectively); and diffusion (J_{0d}; curves *5* ($A_d = 3$) and *10* ($A_d = 1$) for TJ and SJ PVCs, respectively). The values of J_{0t}, J_{0r}, J_{0d}, and series resistance R_s of the PVC structure are given in the table. Curves *2* and *7* in Fig. 2, *a* are the forward dark CVCs of PVCs calculated based on the parameters obtained by fitting. The observed tripling of diode coefficients A_i of the dominant current transport mechanisms in the TJ PVC is indicative of the presence of three photoactive $p-i-n$ junctions, which have equal photocurrent generation capacities, in the monolithic structure. The lack of exponential sections corresponding to

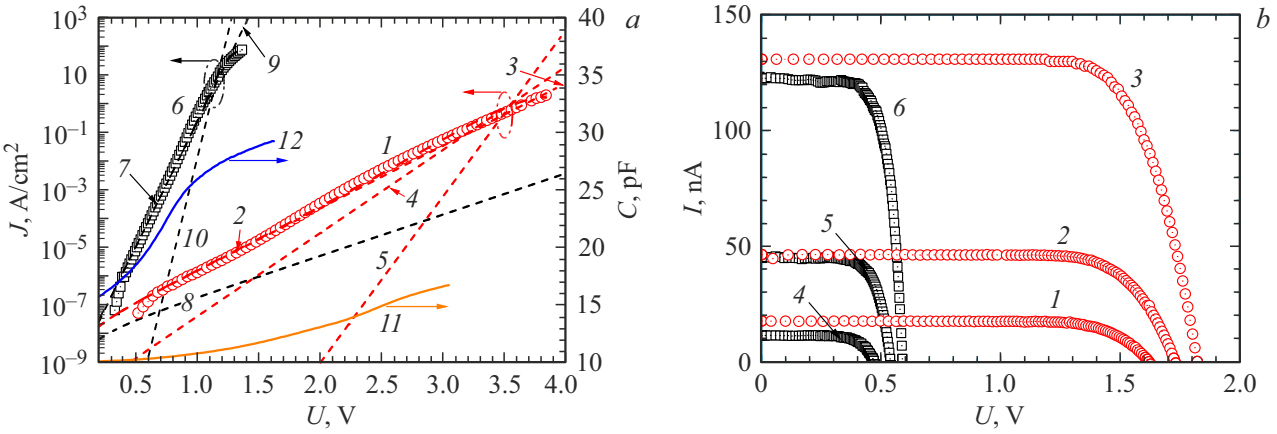

Figure 2. *a* — Experimental (*1*, *6*, *11*, *12*) and calculated (*2*–*5*, *7*–*10*) forward dark CVCs and CVRs of triple-junction (*1*–*5*, *11*) and single-junction (*6*–*10*, *12*) p–i–n PVCs. *b* — Load (light) CVCs of triple-junction (*1*–*3*) and single-junction (*4*–*6*) p–i–n PVCs under illumination by laser radiation ($\lambda = 850$ nm) with a power of 128 (*1*, *5*), 342 (*2*, *6*), 971 (*3*), and 32 nW (*4*).

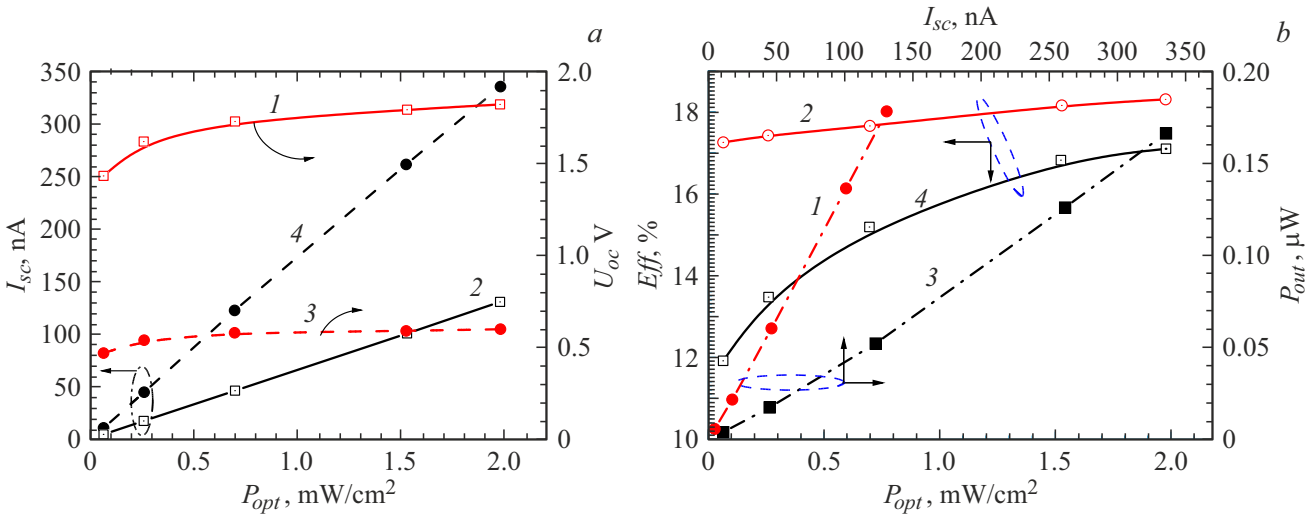

Figure 3. *a* — Dependences of open-circuit voltage U_{oc} (*1*, *3*) and short-circuit current I_{sc} (*2*, *4*) of monolithic triple-junction (*1*, *2*) and single-junction (*3*, *4*) p–i–n PVCs on the optical excitation power ($\lambda = 850$ nm). *b* — Dependences of the output electrical power (*1*, *3*) and efficiency (Eff) (*2*, *4*) of triple-junction (*1*, *2*) and single-junction (*3*, *4*) p–i–n PVCs on the photocurrent.

mixed (tunnel-trap and recombination or recombination and diffusion) current transport mechanisms in the experimental CVCs is attributable to the fact that the CVCs of each TJ PVC subcell are identical. In addition, the lack of „S-shaped“ features in the forward dark CVCs of the TJ PVC indicates that the characteristics of connecting tunnel diodes are close and the tunnel mechanism of current transport is dominant within the operating voltage range. Series resistance R_s of the TJ PVC is two orders of magnitude higher than the one of the SJ PVC (see the table). It should be noted that „saturation“ current J_{0d}, which largely determines the efficiency of PVCs in the photovoltaic mode [12], for the TJ PVC is almost an order of magnitude lower (see the table). The CVRs of both types of samples were measured on the epitaxial wafer at a frequency of 0.1 MHz. The experimental CVRs are shown in Fig. 2, *a* (curves *11* and *12* for TJ and SJ PVCs, respectively). The capacitance of the TJ PVC at a forward bias voltage $\geqslant 1.5$ V is $C = 12$ pF, which is ~ 2.5 times lower than the corresponding value for the SJ PVC.

The load current–voltage curves of SJ and TJ PVCs were measured with continuous monochromatic radiation ($\lambda = 850$ nm) with a power $\leqslant 2$ mW/cm^2 input from a 200 μm optical fiber. The measured load CVCs and calculated photovoltaic parameters for PVCs are presented in Figs. 2, *b* and 3. According to the dependences presented in Fig. 3, *a*, the open-circuit voltage (U_{oc}) for the TJ PVC is ~ 3 times higher than the corresponding voltage for the SJ PVC (curves *1*, *3*), while the short-circuit current (I_{sc}) for the triple-junction PVC is almost 3 times lower than I_{sc} for the SJ PVC (curves *2*, *4*). These relations are maintained throughout almost the entire range of laser radiation power; at ~ 2 mW/cm^2, the open-circuit voltage is $U_{oc} = 1.82$ V for the TJ PVC and $U_{oc} = 0.59$ V for

the SJ PVC (Fig. 3, *a*). The generation of a higher output electrical power at significantly lower photocurrent values is an important advantage of the monolithic triple-junction $p-i-n$ AlGaAs/GaAs PVC structure over the single-junction PVC. Figure 3, *b* presents the dependences of the output electrical power (curves *1*, *3*) and efficiency (curves *2*, *4*) on the photocurrent for TJ and SJ PVCs. Specific output electrical power $P_{out} = 0.34\,\text{mW/cm}^2$ for the triple-junction $p-i-n$ PVC was obtained at photocurrent $J_{sc} = 0.25\,\text{mA/cm}^2$ and an efficiency of 18.3%, while the SJ PVC may achieve the same power at a higher photocurrent density ($J_{sc} = 0.7\,\text{mA/cm}^2$) and a lower efficiency (17%) (Fig. 3). The obtained results indicate that the efficiency of the triple-junction $p-i-n$ AlGaAs/GaAs PVC converting radiation with wavelength $\lambda = 850\,\text{nm}$ at power levels below $2\,\text{mW/cm}^2$ is higher than the efficiency of the single-junction $p-i-n$ AlGaAs/GaAs PVC, while the corresponding operating photocurrent density of the TJ PVC is significantly (approximately 3 times) lower.

Epitaxial structures of monolithic triple-junction $p-i-n$ AlGaAs/GaAs PVCs have been grown by MBE for the first time. At power density $\leqslant 2\,\text{mW/cm}^2$ of laser radiation with wavelength $\lambda = 850\,\text{nm}$, these PVCs provided an open-circuit voltage of 1.82 V and an electrical power of $0.34\,\text{mW/cm}^2$ at an efficiency of 18.3%. The obtained parameter values exceed significantly the characteristics of single-junction $p-i-n$ AlGaAs/GaAs PVCs with the same chip geometry grown by MBE and processed under the same conditions and process parameters.

Conflict of interest

The authors declare that they have no conflict of interest.

References

[1] P. Bhatti, Sci. Transl. Med., **7**, 287ec75 (2015). DOI: 10.1126/scitransalmed.aab3974
[2] H. Helmers, C. Armbruster, M. von Ravenstein, D. Derix, C. Schöner, IEEE Trans. Power Electron., **35**, 7904 (2020). DOI: 10.1109/TPEL.2020.2967475
[3] S. Fafard, F. Proulx, M.C.A. York, L.S. Richard, P.O. Provost, R. Ares, V. Amez, D.P. Masson, Appl. Phys. Lett., **109**, 131107 (2016). DOI: 10.1063/1.4964120
[4] M.C.A. York, S. Fafard, J. Phys. D: Appl. Phys., **50**, 173003 (2017). DOI: 10.1088/1361-6463/aa60a6
[5] J. Huang, Y. Sun, Y. Zhao, S. Yu, J. Dong, J. Xue, C. Xue, J. Wang, Y. Lu, Y. Ding, J. Semicond., **39**, 044003 (2018). DOI: 10.1088/1674-4926/39/9/094006
[6] A. Wang, J. Yin, S. Yu, Y. Sun, Appl. Phys. Lett., **121**, 233901 (2022). DOI: 10.1063/5.0109587
[7] Y. Hanein, J. Goding, APL Bioeng., **8**, 020401 (2024). DOI: 10.1063/5.0209537
[8] K.K. Prudchenko, I.A. Tolkachev, E.V. Kontrosh, E.A. Silantieva, V.S. Kalinovskii, Tech. Phys., **67** (12), 1632 (2022). DOI: 10.21883/TP.2022.12.55199.199-22.
[9] S.N. Bocharov, A.I. Isakov, Yu.Yu. Petrov, K.N. Orekhova, E.V. Dementeva, B.E. Burakov, M.V. Zamoryanskaya, Diam. Relat. Mater., **120**, 108658 (2021). DOI: 10.1016/j.diamond
[10] C. Zhou, J. Zhang, X. Wang, Y. Yang, P. Xu, P. Li, L. Zhang, Z. Chen, H. Feng, W. Wu, ECS J. Solid State Sci. Technol., **10**, 027005 (2021). DOI: 10.1149/2162-8777/abe423
[11] V.P. Khvostikov, V.S. Kalinovskii, S.V. Sorokina, O.A. Khvostikova, V.M. Andreev, Tech. Phys. Lett., **45** (12), 1197 (2019). DOI: 10.1134/S1063785019120083.
[12] V.S. Kalinovskiy, E.V. Kontrosh, G.A. Gusev, A.N. Sumarokov, G.V. Klimko, S.V. Ivanov, V.S. Yuferev, T.S. Tabarov, V.M. Andreev, J. Phys.: Conf. Ser., **993**, 012029 (2018). DOI: 10.1088/1742-6596/993/1/01202

Translated by D.Safin